Article No.: 2097-096X(2025)04-0449-11

Effect of stochastic fracture surface roughness on water flow and heat transfer in fractured rocks

LIU Dongdong[1], SONG Wenjie[2], LU Wei[2], ZHONG Guo[1], YANG Tao[1]
(1. *Guangzhou Railway Polytechnic*, *Guangdong Guangzhou*, 511300, *China*;
2. *China Institute of Water Resources and Hydropower Research*, *Beijing*, 100038, *China*)

Abstract: As the dominant seepage channel in rock masses, it is of great significance to study the influence of fracture roughness distribution on seepage and heat transfer in rock masses. In this paper, the fracture roughness distribution functions of the Bakhtiary dam site and Oskarshamn/Forsmark mountain were fitted using statistical methods. The COMSOL Multiphysics finite element software was utilized to analyze the effects of fracture roughness distribution types and empirical formulas for fracture hydraulic aperture on the seepage field and temperature field of rock masses. The results show that: (1) The fracture roughness at the Bakhtiary dam site and Oskarshamn/Forsmark mountain follows lognormal and normal distributions, respectively; (2) For rock masses with the same expected value and standard deviation of fracture roughness, the outflow from rock masses with lognormal distribution of fracture roughness is significantly larger than that of rock masses with normal distribution of fracture roughness; (3) The fracture hydraulic aperture, outflow, and cold front distance of the Li and Jiang model are significantly larger than those of the Barton model; (4) The outflow, hydraulic pressure distribution, and temperature distribution of the Barton model are more sensitive to the fracture roughness distribution type than those of the Li and Jiang model.

Keywords: discrete fracture networks; roughness distribution; hydro-mechanical aperture model; seepage and heat transfer

Chinese Library Classification No.: TU452 **Document code**: A **doi**: 10.13244/j.cnki.jiwhr.20240245

1 Introduction

Accurate estimation of water flow in fractured rocks is crucial for numerous rock engineering projects, including enhanced geothermal systems[1], hazardous waste disposal[2], oil exploitation[3] and tunnel grouting[4]. Compared to the rock matrix, fractures are generally more permeable and are considered the predominant fluid pathways in fractured rocks[5]. Fractures are commonly conceptualized as two smooth parallel plates with a constant aperture[6]. In fact, fracture surfaces are generally uneven rough[7]. Therefore, accurate representation of fracture geometry is essential for accurately analyzing fluid and solute transfer in fractured rocks[8]. In the quantization process of *JRC* (Joint Roughness Coefficient), fracture surface roughness data must be obtained and digitized. Efforts to quantify fracture surface roughness are summarized in chronological order[9]. Various parameters are used to describe fracture surface roughness, such as fractal dimension, *JRC*, mean asperity height, sharpness of surface peaks, surface first derivative, surface tortuosity coefficient, root-mean-square of asperity height, roughness anisotropy, mean asperity height plane, root-mean-square asper-

Received: 2024-12-10; Published Online: 2025-07-11
Available Online: https://link.cnki.net/urlid/10.1788.TV.20250711.1120.002
Supported by: College Students Innovation and Entrepreneurship Project of Guangzhou Railway Polytechnic (2025CXCY015)
About the Author: Liu Dongdong(1992-), Ph.D., lecture of engineering, engaged in the research on the geomaterial multiphysics coupling and tunnel excavation stability. E-mail: dond_liu@126.com
Corresponding Author: Song Wenjie(1986-), Ph.D., senior engineer of engineering, engaged in hydraulic structure monitoring and tunnel excavation stability. E-mail: songwj@iwhr.com

ity height, roughness spatial variations, Hurst exponent, mean inclination angle, and peak asperity height.

Experimental investigations demonstrate that fracture surface roughness significantly impacts the thermal, hydraulic, mechanical, and solute transport behaviors of a single fracture[10-11]. The fundamental choice for macroscopic process simulation in fractured rock masses is to explicitly or implicitly represent fractures. The discrete fracture network (DFN) model, as an explicit conceptual model, is widely adopted to investigate the thermo-hydro-mechanical-chemical (THMC) coupling processes in fractured rocks at the field scale[12]. For simplicity, most numerical studies assume identical hydraulic and mechanical fracture apertures, meaning the reduction in fracture hydraulic aperture due to fracture surface roughness is not properly considered[13]. Heretofore, little is known about how the reduction in fracture hydraulic aperture affects 3D macroscopic heat and mass transfer in complex fractured rocks with stochastic fracture surface roughness[14]. Fracture hydraulic aperture can be categorized into modified and local models. The modified model globally estimates the effects of overall fracture geometric characteristics, while the local model evaluates the influences of fracture segment geometrical features[15]. In numerous 3D simulation models, fractures are represented by 2D planes with a single modified fracture hydraulic aperture. Many modified models estimate fracture hydraulic aperture based on the fracture mechanical aperture[16]. For a single fracture, different modified models can generate different hydraulic apertures. However, little is known about how the fracture hydro-mechanical aperture relationship impacts 3D macroscopic heat and mass transfer in complex fractured rocks with stochastic fracture surface roughness.

In this paper, published *JRC* data from the Bakhtiary dam site and Oskarshamn/Forsmark mountain are reviewed to obtain fracture surface roughness distribution functions. The impacts of these two fracture surface roughness distribution types and two fracture hydro-mechanical models on 3D macroscopic water flow and heat transfer are investigated using the finite element software COMSOL Multiphysics.

2 DFN Model

2.1 Fracture surface roughness distribution Due to the difficulty of obtaining in-situ data, little attention has been paid to the *JRC* distribution in the field. Two sets of *JRC* data were reported: 106 *JRC* data collected at the Bakhtiary dam site[17] and 176 *JRC* data assembled at the Oskarshamn/Forsmark mountain[18]. The empirical cumulative distribution function (ecdf) in MATLAB is used to estimate the JRC distribution of the two sites. The fitting effects are evaluated by the chi-square goodness-of-fit test, expressed as:

$$\chi^2 = \sum_{i=1}^{k} \frac{(Q_i - E_i)}{E_i} \tag{1}$$

where k is the number of value partition bins, i the bin order number, Q the observed frequency, and E the expected frequency.

The *JRC* distribution of the two sites is presented in Fig.1, along with respective chi-square values. The *JRC* at the Bakhtiary dam site is fitted to a lognormal distribution with a chi-square value of 4.43, and the *JRC* at the Oskarshamn/Forsmark mountain is fitted to a normal distribution with a chi-square value of 3.82. These chi-square values indicate that the two *JRC* distribution functions are appropriate. The fitting parameters in Table 1 suggest that *JRC* distribution depends to some extent on the site's geological conditions. Here, both distribution functions are selected to investigate the influences of *JRC* distribution on 3D macroscopic heat and mass transfer in fractured rocks.

2.2 Fracture hydro-mechanical aperture relationship Due to surface roughness, the fracture hydraulic aperture is commonly smaller than the fracture mechanical aperture. Table 2 shows the main modified models of

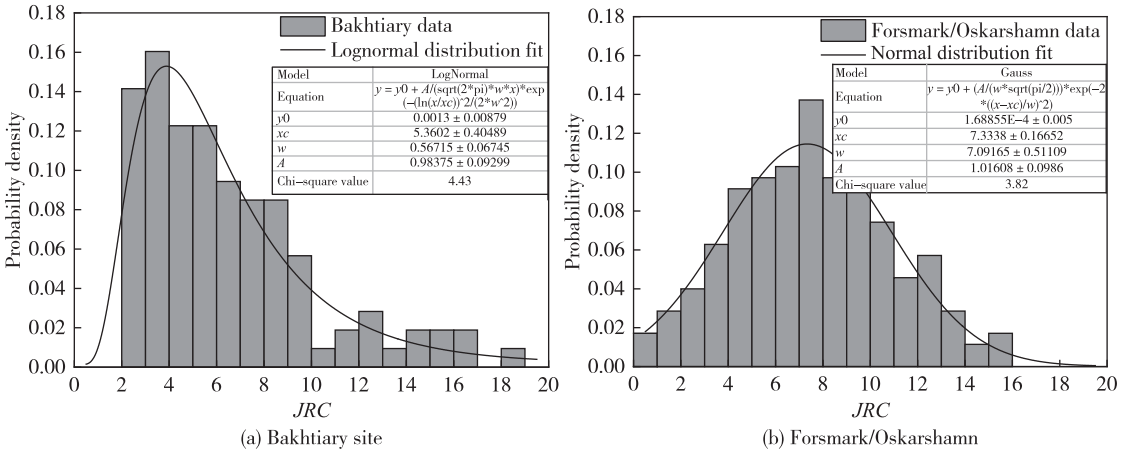

(a) Bakhtiary site (b) Forsmark/Oskarshamn

Fig. 1 *JRC* observation values and fitting results of fractures in different sites

Table 1 Fitting parameters of *JRC* distribution at two sites

Fields	Distribution types	Mean value	Standard deviation
Bakhtiary	Lognormal distribution	1.68	0.57
Oskarshamn/Forsmark	Normal distribution	7.33	3.55

Table 2 Fracture hydro-mechanical aperture relationship models

Authors	Equations of e/E	Description of symbol
Patir and Cheng[19]	$\left(1-0.9e^{-0.56E/\sigma_E}\right)^{1/3}$	E is the mechanical aperture.
Barton et al.[20]	$\left(e/JRC^{2.5}\right)^{1/2}$	σ_E is the mechanical aperture standard deviation.
Renshaw[21]	$\left(1+\sigma_E^2/E^2\right)^{-1/2}$	E is the mechanical aperture harmonic mean.
Zimmerman and Bodvarsson[22]	$\left(1-1.5\sigma_E^2/E^2+\cdots\right)^{1/3}$	τ is the tortuosity.
Waite et al.[23]	$E/\tau^{1/3}$	JRC_{mob} is the JRC mobilized value.
Olsson and Barton[24]	$\begin{cases}\left(e/JRC^{2.5}\right)^{1/2} & u_s \leqslant 0.75u_{sp}\\ JRC_{\mathrm{mob}}^2/e & u_s > 0.75u_{sp}\end{cases}$	u_s is the shear displacement.
Rasouli and Hosseinian[25]	$\left(1-0.03d_{\mathrm{mc}}^{-0.565}\right)^{JRC/3}$ or $\left(1-2.25\sigma_E/E\right)^{1/3}$	u_{sp} is the peak shear displacement.
Xiong et al.[26]	$\left[\left(1-\frac{\sigma_E}{E}\right)\left(1-\frac{\sigma_E\sqrt{\sigma_{\mathrm{slope}}Re}}{10E}\right)\right]^{1/3}$	d_{mc} is the minimum closure distance.
Li and Jiang[27]	$\begin{cases}\dfrac{1}{1+Z_2^{2.25}} & Re<1\\ \dfrac{1}{1+Z_2^{2.25}+(6+40Z_2^{2.25})(Re-1)\cdot 10^{-5}} & Re\geqslant 1\end{cases}$	JRC_a is the average JRC.
Xie et al.[28]	$\left(0.94-\frac{\sigma_E^2}{E^2}\right)^{1/3}$	σ_{slope} is the standard deviation of fracture surface local slope.
		Re is the Reynolds number.
		Z_2 is the root mean square of the profile first deviation.

the fracture hydro-mechanical aperture relationship. These modified models are based on the analysis of different rock fractures. Fig.2 exhibits some models that are prone to significantly different results: (1) Relatively minor influences of fracture surface roughness on fracture hydraulic aperture are observed with three models developed by Patir and Cheng[19], Renshaw[21] and Li and Jiang[27]; (2) For small *JRC*, unrealistic results are possibly predicted with two models proposed by Barton et al[20] and Olsson and Barton[24]; (3) For large

JRC, negative results are potentially obtained with two models provided by Zimmerman and Bodvarsson[22] and Rasouli and Hosseinian[25]. The main reasons for the significant differences between model results include: (1) These models are constructed based on specific roughness ranges rather than a general roughness range; (2) Significant inertial effects of fluid at high Reynolds numbers are not considered, except for the models proposed by Xiong et al[26]. and Li and Jiang[27]. In terms of local models, various calculation methods have been developed[28-29]. However, the fracture hydraulic aperture in a DFN with numerous fractures is very difficult to describe. In this paper, only the effects of global models are discussed.

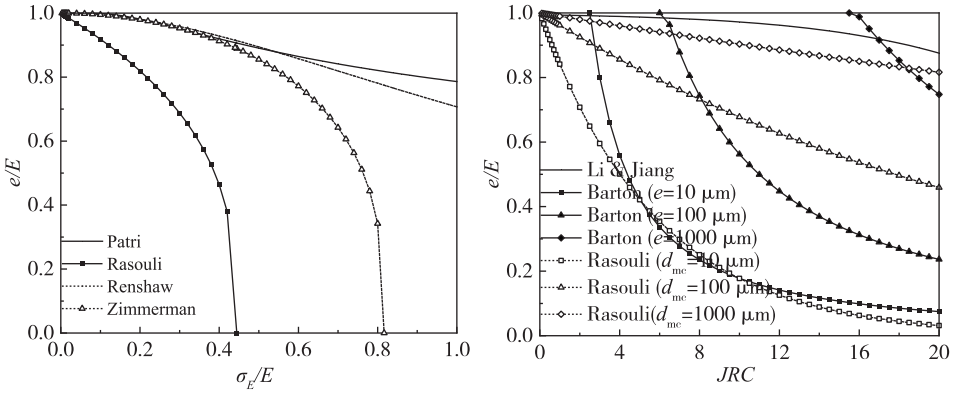

Fig. 2 Comparison of different fracture hydro-mechanical aperture relationship models

2.3 DFN model establishment The representative elementary volume side of the fractured rocks at the Sellafield area, UK, is 5 m[30]. In this paper, a square DFN model with a 5 m side length was built based on the Sellafield area fracture parameters, including density, center, diameter, strike angle, and dip direction angle. Some assumptions are made: the fracture mechanical apertures are identical; the fracture geometries are circular; the fracture centers, diameters, dips, and dip angles follow uniform distribution, exponential distribution, Fisher distribution, and Fisher distribution, respectively. The values of fracture geometric features are listed in Table 3.

Table 3 Fracture geometric features

Geometric features	Statistic distribution	Parameters		Value
Mechanical aperture				60μm
Fracture density				0.6m^3
Fracture center	Uniform distribution			
Fracture diameter	Exponential distribution	Mean value	2.0m	0.8 ~ 4.0m
Fracture strike angle	Fisher distribution	Mean value	0°	0 ~ 360°
		Fisher constant	0.5	
Fracture dip direction angle	Fisher distribution	Mean value	30°	0 ~ 90°
		Fisher constant	2	

The research domain should be determined before the DFN establishment. If the DFN is directly built in the research domain, only the fractures with centers located in the research domain will be generated, while the fractures with centers located outside the study domain and with parts extended to the interest domain will be neglected. As a result, the fracture density near the domain boundary may decrease. Therefore, the DFN should first be constructed in a large domain and then truncated to the interest domain. The schematic of a 3D DFN is presented in Fig.3. The right DFN is truncated from the left one.

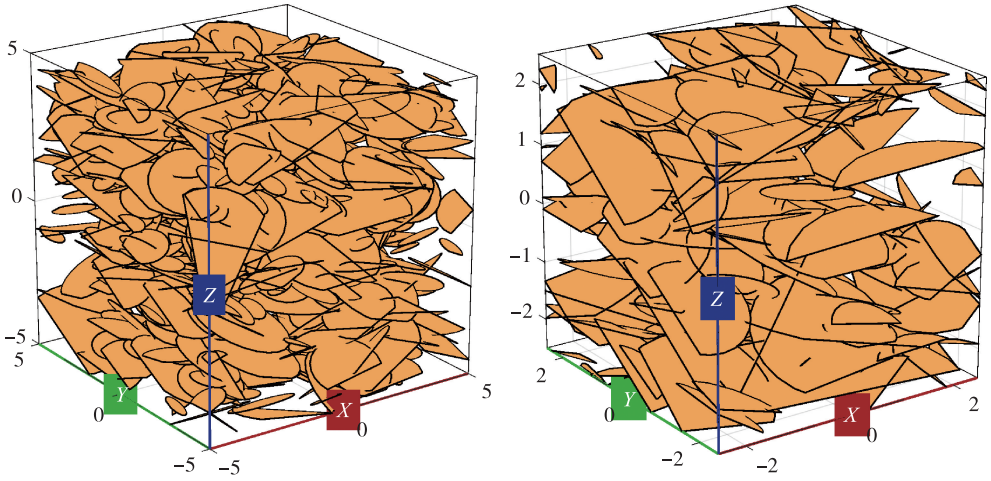

(a) Before truncation (b) After truncation

Fig. 3 DFN model comparison

For fractures with identical mechanical apertures, different fracture surface roughness may induce various hydraulic apertures, resulting in large errors in the seepage and temperature fields of fractured rocks. The *JRC* distribution is described by the normal distribution and lognormal distribution in Section 2. The fracture hydraulic aperture is estimated based on the two hydro-mechanical aperture models proposed by Barton and Li and Jiang. The relationship between Z_2 and *JRC* was provided by Tse and Curden[31]. To systematically investigate the influences of fracture surface roughness, four cases listed in Table 4 are considered in this work. Cases 1 and 2 are arranged based on the*JRC* distribution at the Bakhtiary dam site and Oskarshamn/Forsmark mountain, respectively. To study the effects of *JRC* distribution types, case 3 shares the mean and standard deviation of case 2. Case 4 neglects the fracture surface roughness to serve as a reference. The schematics of *JRC* distribution are exhibited in Fig.4.

Table 4 Parameters of different *JRC* distribution

Cases	Distribution types	Mean value	Standard deviation
1	Lognormal distribution	1.68	0.57
2	Normal distribution	7.33	3.55
3	Lognormal distribution	1.89	0.46

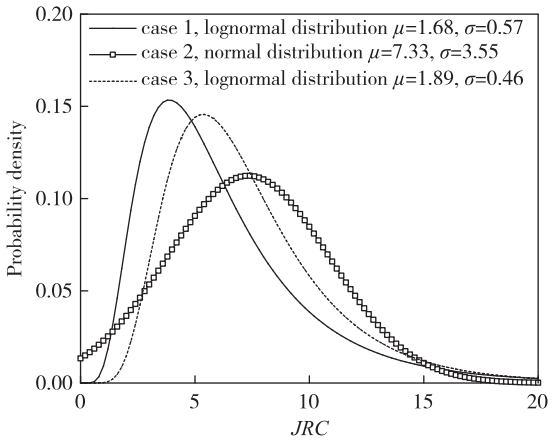

Fig. 4 *JRC* distribution functions

To directly observe the distribution of fracture hydraulic apertures, the pipe element model is used to simplify the planar fracture into a linear one, and thus the pipe diameter can reflect the fracture aperture to some extent. Fig.5 shows the pipe element distribution of four cases. Compared with the Barton model, the Li and Jiang model usually gives larger hydraulic apertures. For the first three cases applied with the same fracture hydro-mechanical aperture model, the hydraulic apertures of the same fracture may differ due to disparate *JRC* distributions.

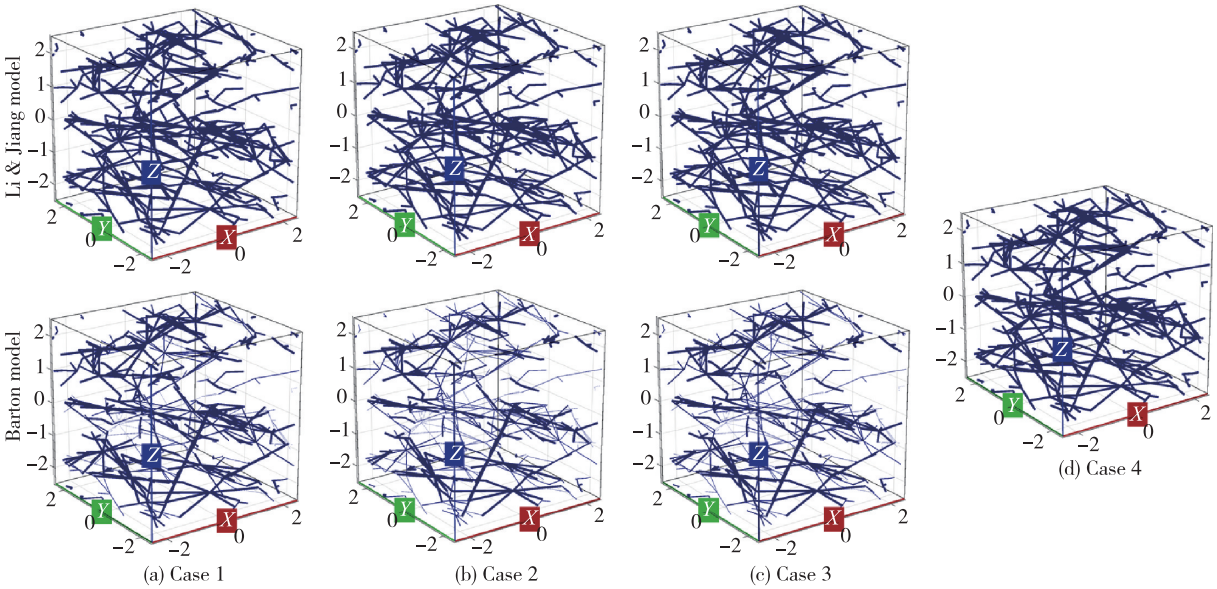

Fig. 5 Pipe element distribution with disparate *JRC* distribution and different *e*/*E* models

Fig.6 presents the initial and boundary conditions of water flow and heat transfer in fractured rocks. Some assumptions on the water flow are: the top, bottom, front, and back boundaries are impermeable; the water pressures at the left and right boundaries are 10^6 Pa and 0 Pa, respectively; the initial water pressure across the research domain is 0 Pa. Some hypotheses on the heat transfer are: the top, bottom, front, back, and right boundaries are adiabatic, and the initial temperature throughout the interest domain is 90 ℃. 20 ℃ cold water is injected from the left boundary. Parameters of rock and water are listed in Table 5.

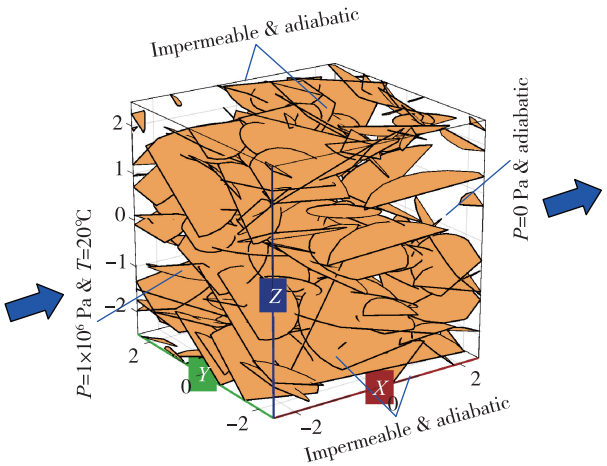

Fig. 6 Initial and boundary conditions in a DFN model

Table 5 Parameters of rock and water

Parameters	Value	Parameters	Value
Water density	1000kg/m^3	Rock density	2650kg/m^3
Water dynamic viscosity	0.001Pa·s	Rock conductivity	3W/(m·K)
Water conductivity	0.5W/(m·K)	Rock heat capacity	1000J/(kg·K)
Water heat capacity	4200J/(kg·K)		

3 Simulation and Results

3.1 Water flow and heat transfer equations COMSOL Multiphysics is employed to simulate water flow and heat transfer processes in crystalline fractured rocks. The heat convection in the rock matrix is neglected due to its significantly lower permeability compared to fractures. The local thermal equilibrium is applied to describe the heat exchange between fracture water and the rock matrix[32]. The heat transfer in the rock matrix is governed by heat conduction, expressed as:

$$\rho_r c_r \frac{dT}{dt} - \lambda_r \left(\frac{\partial^2 T}{\partial x^2} + \frac{\partial^2 T}{\partial y^2} + \frac{\partial^2 T}{\partial z^2} \right) = 0 \tag{2}$$

where t is denotes time, T denotes temperature, ρ_r the rock density, c_r the rock heat capacity, and λ_r the rock heat conduction coefficient.

The pressure and temperature of fracture water are assumed to be constant in the normal direction of the fracture surface. The governing equations for fracture water flow and heat transfer are:

$$\frac{e^3}{12\eta} \left(\frac{\partial^2 P}{\partial x^2} + \frac{\partial^2 P}{\partial y^2} + \frac{\partial^2 P}{\partial z^2} \right) = 0 \tag{3}$$

$$e\rho_f c_f \frac{dT}{dt} + \frac{e^3 \rho_f c_f}{12\eta} \left(\frac{\partial P}{\partial x} \cdot \frac{\partial T}{\partial x} + \frac{\partial P}{\partial y} \cdot \frac{\partial T}{\partial y} + \frac{\partial P}{\partial z} \cdot \frac{\partial T}{\partial z} \right) - e\lambda_f \left(\frac{\partial^2 T}{\partial x^2} + \frac{\partial^2 T}{\partial y^2} + \frac{\partial^2 T}{\partial z^2} \right) = f_{upper} + f_{lower} \tag{4}$$

where P is the water pressure, e the fracture hydraulic aperture, ρ_f the water density, c_f the water heat capacity, λ_f the water heat conduction coefficient, η the water dynamic viscosity, f_{upper} the heat exchange between the upper fracture surface and rock matrix, and f_{lower} the heat exchange between the lower fracture surface and rock matrix.

In the above governing equations, sources and constraints are added with weak form contributions. Fractures and the rock matrix are discretized by triangle and tetrahedral elements, respectively. The spatio-temporal deviation terms are handled by the implicit backward differentiation formulas. The linear system is solved by the parallel direct sparse solver interface in COMSOL Multiphysics.

3.2 Water flow simulation results First, DFNs with a mechanical aperture of 60 μm are used to investigate the influence of fracture surface roughness on water flow. Second, DFNs with mechanical apertures of 6 μm, 60 μm, and 600 μm are utilized to reveal the impacts of fracture mechanical aperture on water flow.

In Fig.7, the flow rates of four cases are normalized by the flow rate of case 4. Unaffected by fracture surface roughness, the flow rate of case 4 is the largest of the four cases. The flow rates in DFNs with *JRC* lognormal distribution are greater than those in DFNs with JRC normal distribution. For cases 1, 2, and 3, the normalized flow rates calculated by the Li and Jiang model are 96.5%, 95.9%, and 96.1%, respectively, whereas the normalized flow rates estimated by the Barton model are 47.9%, 40.1%, and 41.9%, respectively. The flow rates of the Barton model are more sensitive to *JRC* distribution parameters than those of the Li and Jiang model, i.e., a small mean deviation (1.02) of *JRC* between two lognormal distributions causes significantly disparate flow rates by comparing the results of cases 1 and 3, whereas relatively small flow rate differences exist between differ-

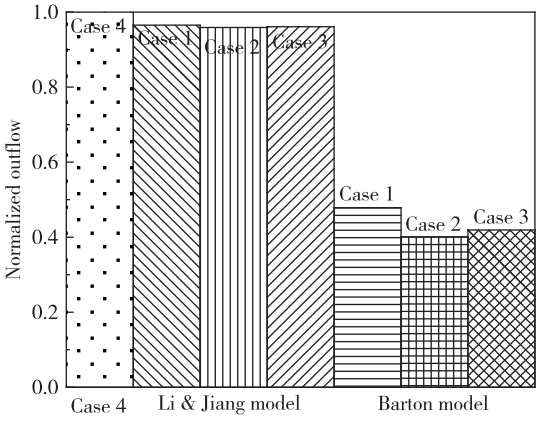

Fig. 7 Comparison between normalized outflow for different cases

ent *JRC* distributions with identical mean and variance by comparing the results of cases 2 and 3. For the Li and Jiang model, individual flow rates approximate those of case 4, and slight differences exist between the flow rates of the first three cases. This demonstrates that the flow rate of the Li and Jiang model is not obviously influenced by the *JRC* distribution type. Fig.8 illustrates the water pressure nephograms of the four cases. The water pressure distribution in the Barton model is more sensitive to *JRC* distribution parameters compared with that in the Li and Jiang model.

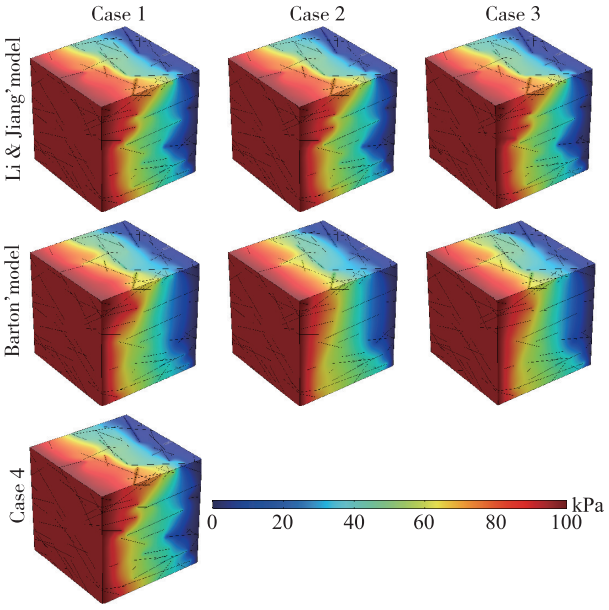

Fig. 8 Water pressure in fractured rocks with disparate *JRC* distribution and different *e*/*E* models

Table 6 lists the flow rates of various DFNs with different mechanical apertures. The flow rates in the Barton model with a 600 μm fracture mechanical aperture are almost unaffected by the fracture surface roughness, while the flow rates of DFNs with a 60 μm fracture mechanical aperture dramatically decrease due to the fracture surface roughness. The reason can be described by the fact exhibited in Fig.2(right) that the influences of fracture surface roughness on hydraulic aperture become less for larger mechanical apertures in the Barton model. By contrast, the flow rates in the Li and Jiang model are insignificantly affected by the fracture surface roughness due to the independence of the hydro-mechanical aperture relationship on mechanical aperture (Fig.2).

3.3 Heat transfer simulation results The 60 μm fracture mechanical aperture is used to study the impacts of fracture surface roughness on heat transfer. Fig.9 displays the temperature nephograms of the four cases at the simulation time of 2×10^6 s. The low-temperature regions in DFNs with *JRC* lognormal distribution are slightly larger than those in DFNs with *JRC* normal distribution. In other words, the cold front moves faster in DFNs with *JRC* lognormal distribution. In comparison with the temperature distribution in the Li and Jiang model, the cold front moves more slowly in the Barton model due to the smaller hydraulic aperture estimated. Somewhat differences in temperature distribution exist in the Barton model, whereas barely any deviations occur in the Li and Jiang model. Consequently, the heat transfer in fractured rocks depends largely on the fracture hydro-mechanical relationship.

4 Conclusions

Based on the published fracture hydro-mechanical aperture relationship and estimated *JRC* distribution,

Table 6 Flow rates of various DFNs with different mechanical apertures

Mechanical apertures/μm	Model types	Cases	Flow rates×10^{-6}/(m^3/s)
6	Barton model	Case 1	1.50
		Case 2	1.50
		Case 3	1.50
	Li and Jiang model	Case 1	1.51
		Case 2	1.51
		Case 3	1.51
	—	Case 4	1.51
60	Barton model	Case 1	2.34
		Case 2	1.69
		Case 3	2.05
	Li and Jiang model	Case 1	4.72
		Case 2	4.69
		Case 3	4.70
	—	Case 4	4.89
600	Barton model	Case 1	2390
		Case 2	2410
		Case 3	2380
	Li and Jiang model	Case 1	2340
		Case 2	2410
		Case 3	2320
	—	Case 4	2470

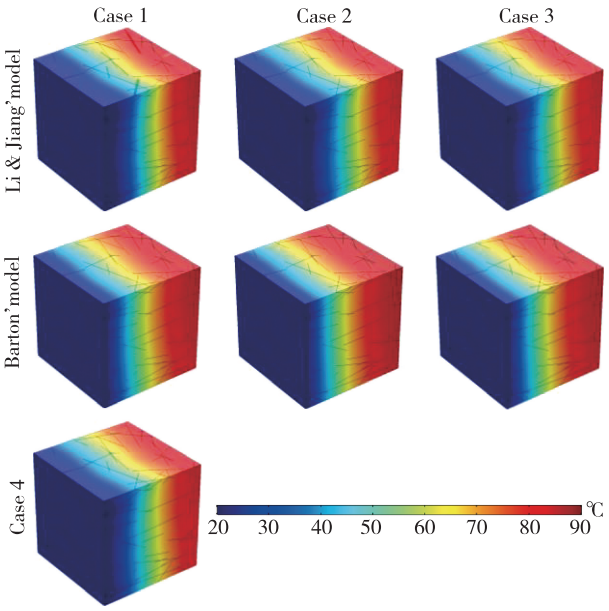

Fig. 9 Fractured rock temperature for different *JRC* distribution and different *e*/*E* models

the influences of *JRC* on the 3D macroscopic water flow and heat transfer in fractured rocks were investigated using the finite element software COMSOL Multiphysics. Numerical results indicate that both the flow rate and temperature are significantly affected by the fracture hydro-mechanical aperture models and *JRC* distribution

types. Some conclusions are summarized as:

(1) Lognormal distribution and normal distribution are adopted to appropriately describe the *JRC* distribution at the Bakhtiary dam site and Oskarshamn/Forsmark mountain, respectively. For rock mass with the same expected value and standard deviation of fracture roughness, the fractured rocks with *JRC* lognormal distribution are more permeable than those with *JRC* normal distribution, thus the cold front moves faster in the DFN with *JRC* lognormal distribution than that with *JRC* normal distribution.

(2) Due to the greater fracture hydraulic aperture obtained by the Li and Jiang model, the outflow and cold front distance of the Li and Jiang model are significantly larger than those of the Barton model. Therefore, an appropriate hydro-mechanical aperture relationship should be selected to correctly analyze the water flow and heat transfer processes in fractured rocks.

(3) For different *JRC* distribution parameters, there are greater differences in the water outflow, water pressure distribution, and temperature distribution in the Barton model, indicating that the water flow and heat transfer processes in the Barton model are more sensitive to *JRC* distribution than those in the Li and Jiang model.

References:

[1] CAO W, HUANG W, CHEN J, et al. Numerical study on the heat extraction performance of enhanced geothermal systems with a well-fracture-reservoir combined model[J]. Renewable Energy, 2023, 202: 370-380.

[2] ZHANG X, MA F, DAI Z, et al. Soltanian, radionuclide transport in multi-scale fractured rocks: A review[J]. Journal of Hazardous Materials, 2022, 424: 127550.

[3] WANG D, CHENG L, CAO R, et al. The effects of the boundary layer and fracture networks on the water huff-n-puff process of tight oil reservoirs[J]. Journal of Petroleum Science and Engineering, 2019, 176: 466-480.

[4] DOU J, ZHAO W, LU W, et al. Study on high-pressure grouting fluid diffusion process in complex fractured surrounding rock of water diversion tunnel[J]. Journal of China Institute of Water Resources and Hydropower Research, 2023, 21(6): 565-573. (in Chinese)

[5] WANG J, WANG Z. Study on one-dimensional ring unit model for determining the permeability coefficient tensor of fractured rock masses[J]. Journal of Hydraulic Engineering, 2023, 54(5): 575-586. (in Chinese)

[6] SHA S, ZHANG G. Simulation of 3D hydraulic fracturing of concrete gravity dams based on stress-seepage damage coupling model[J]. Journal of China Institute of Water Resources and Hydropower Research, 2020, 18(1): 1-11. (in Chinese)

[7] GAN L, MA H, SHEN Z. Roughness characterization of concave fracture surface and coefficient fitting of modified cubic law[J]. Journal of Hydraulic Engineering, 2021, 52(4): 420-431. (in Chinese)

[8] ZHONG Z, DING J. HU Y. Size effect on the hydraulic behavior of fluid flow through rough walled fractures: a case of radial flow[J]. Hydrogeology Journal, 2022, 30: 97-109.

[9] WANG M, CHEN Y, MA G, et al. Influence of surface roughness on nonlinear flow behaviors in 3D self-affine rough fractures: Lattice Boltzmann simulations[J]. Advances in Water Resources, 2016, 96: 373-388.

[10] TIAN X, YE Z, LUO W. Effect of rock fracture geometry on its seepage and heat transfer characteristics[J]. Rock and Soil Mechanics, 2023, 44(12): 3512-3521. (in Chinese)

[11] ZHAO M, KONG D. Study on seepage characteristics of rock fractures considering fracture surface roughness and opening fractal dimension[J]. Chinese Journal of Rock Mechanics and Engineering, 2022, 41(10): 1993-2002. (in Chinese)

[12] BERRE I, DOSTER F, KEILEGAVLEN E. Flow in fractured porous media: A review of conceptual models and discretization approaches[J]. Transport in Porous Media, 2019, 130: 215-236.

[13] LI X, XU Y. Hydraulic and solute transport coupling model for fractured rock mass with discrete fracture network using computational method[J]. Chinese Journal of Geotechnical Engineering, 2019, 41(6): 1164-1171. (in Chi-

nese)
[14] LUO S, ZHAO Z, PENG H, et al. The role of fracture surface roughness in macroscopic fluid flow and heat transfer in fractured rocks[J]. International Journal of Rock Mechanics and Mining Sciences, 2016, 87: 29-38.
[15] WANG Z, XU C, DOWD P. A modified cubic law for single-phase saturated laminar flow in rough rock fractures [J]. International Journal of Rock Mechanics and Mining Sciences, 2018, 103: 107-115.
[16] CAO C, XU Z, CHAI J, et al. Radial fluid flow regime in a single fracture under high hydraulic pressure during shear process[J]. Journal of Hydrology, 2019, 579: 124142.
[17] SANEI M, FARAMARZI L, Fahimifar A, et al. Shear strength of discontinuities in sedimentary rock masses based on direct shear tests[J]. International Journal of Rock Mechanics and Mining Sciences, 2015, 75: 119-131.
[18] ASADOLLAHI P. Stability Analysis of a Single Three Dimensional Rock Block: Effect of Dilatancy and High-Velocity Water Jet Impact[D]. Austin: University of Texas at Austin, 2009.
[19] PATIR N, CHENG H. An average flow model for determining effects of three-dimensional roughness on partial hydrodynamic lubrication[J]. Journal of Lubrication Technology, 1978, 100: 12-17.
[20] BARTON N, BANDIS S, BAKHTAR K. Strength, deformation and conductivity coupling of rock joints[J]. International Journal of Rock Mechanics and Mining Sciences, 1985, 22: 121-140.
[21] RENSHAW C. On the relationship between mechanical and hydraulic apertures in rough-walled fractures[J]. Journal of Geophysical Research, 1995, 100: 24629-24636.
[22] ZIMMERMAN R, BODVARSSON G. Hydraulic conductivity of rock fractures[J]. Transport in Porous Media, 1996, 23: 1-30.
[23] WAITE M, GE S, SPETZLER H. A new conceptual model for fluid flow in discrete fractures: An experimental and numerical study[J]. Journal of Geophysical Research, 1999, 104: 13049-13059.
[24] OLSSON R, BARTON N. An improved model for hydromechanical coupling during shearing of rock joints[J]. International Journal of Rock Mechanics and Mining Sciences, 2001, 38: 317-329.
[25] RASOULI V, HOSSEINIAN A. Correlations developed for estimation of hydraulic parameters of rough fractures through the simulation of JRC flow channels[J]. Rock Mechanics and Rock Engineering, 2011, 44: 447-461.
[26] XIONG X, LI B, JIANG Y, et al. Experimental and numerical study of the geometrical and hydraulic characteristics of a single rock fracture during shear[J]. International Journal of Rock Mechanics and Mining Sciences, 2011, 48: 1292-1302.
[27] LI B, JIANG Y. Quantitative estimation of fluid flow mechanism in rock fracture taking into account the influences of JRC and Reynolds number[J]. Journal of the Mining and Materials Processing Institute of Japan, 2013, 129: 479-484.
[28] HE X, SINAN M, KWAK H, et al. A corrected cubic law for single-phase laminar flow through rough-walled fractures[J]. Advances in Water Resources, 2021, 154: 103984.
[29] KLEPIKOVA M, MEHEUST Y, ROQUES C, et al. Heat transport by flow through rough rock fractures: a numerical investigation[J]. Advances in Water Resources, 2021, 156: 104042.
[30] ZHAO Z, JING L, NERETNIEKS I, et al. Numerical modeling of stress effects on solute transport in fractured rocks[J]. Computers and Geotechnics, 2011, 38: 113-126.
[31] TSE R, CRUDEN D. Estimating joint roughness coefficients[J]. International Journal of Rock Mechanics and Mining Sciences, 1979, 16: 303-307.
[32] SAHAR H, THOMAS H, BORIS G, et al. Critical review of the local thermal equilibrium assumption in heterogeneous porous media: Dependence on permeability and porosity contrasts[J]. Applied Thermal Engineering, 2019, 147: 962-971.

(Executive editor: LI Na)